Macromolecules
ARTICLE

*Macromolecules* **2009**, *42*, 7465–7473 **7465**
DOI: 10.1021/ma901276c

# Dual Reversible Self-Assembly of PNIPAM-Based Amphiphiles Formed by Inclusion Complexation

**Jiong Zou,[†,‡] Bing Guan,[†] Xiaojuan Liao,[†] Ming Jiang,*[,†] and Fenggang Tao[‡]**

[†]*The Key Laboratory of Molecular Engineering of Polymers and Department of Macromolecular Science, Fudan University, 220 Handan Rd., Shanghai 200433, China, and* [‡]*Department of Chemistry, Fudan University, 220 Handan Rd., Shanghai 200433, China*

*Received June 13, 2009; Revised Manuscript Received August 28, 2009*

ABSTRACT: β-Cyclodextrin (β-CD)-ended linear poly(*N*-isopropylacrylamide) (β-CD-PNIPAM) and Frechét-type benzyl ether dendron with an azobenzene group (G*x*-Azo) at the apex site form noncovalently connected amphiphiles (NCCAs) by inclusion complexation between the azo group and β-CD. The NCCAs self-assemble into vesicles in water. Optical switching of the assembly and disassembly is realized by alternating visible and UV irradiation, which causes the isomerization of the azo groups and their consequent complexation and decomplexation with β-CD. The structure and morphology of the vesicles were characterized by dynamic light scattering (DLS), static light scattering (SLS), SEM, TEM, and AFM. These photoresponsive vesicles can further respond to heat stimuli resulting in reversible aggregation and disaggregation of the vesicles.



## Introduction

In the past decades, poly(*N*-isopropylacrylamide) (PNIPAM) is one of the most studied thermally responsive polymers which exhibits a coil−globule transition in aqueous solutions at its lower critical solution temperature (LCST) around 32 °C.[1−3] Much efforts have been focused on the hydrophobic modification of the PNIPAM chains, which affects significantly the behavior of PNIPAM, leading to new thermo-responsive materials.[4−7] Recently, living free radical polymerizations, such as nitroxide-mediated polymerization (NMP),[8] reversible addition−fragmentation chain transfer (RAFT),[5,9,10] and atom transfer radical polymerization (ATRP),[11] are widely used to build up a series of diblock copolymers comprised of a hydrophilic PNIPAM block and a hydrophobic block. Thus, some of such block copolymers show dual stimuli-responsive properties if the block connected to PNIPAM bears functional groups sensitive to additional environmental changes such as pH,[11,12] light,[13] and ionic strength.[14]

In our long-term research of macromolecular self-assembly, we developed "block copolymer free strategies". In the strategies complementary polymer pairs served building blocks and self-assembled into noncovalently connected micelles (NCCM)[15] or vesicles (NCCV)[16] driven by hydrogen bonding. In parallel with our work in constructing NCCMs from polymer pairs, the research groups of Schubert, Gohy, and O'Reiley have focused on developing supramolecular block copolymers in which the constituent blocks are connected by metal−ligand coordination . The resultant noncovalently connected block copolymers (NCCBs) could self-assemble further into NCCMs or NCCVs.[17] Recently, the host−guest interactions have been successfully used as driving forces in constructing NCCBs.[18] For example, Shi et al.[18b] reported a double hydrophilic block copolymer, which consists of adamentane-ended PNIPAM and β-CD-ended poly(4-vinylpyridine). The two blocks are connected by the inclusion complexation between the β-CD and adamantane. This NCCB was found to be able to form two different NCCMs in response to pH and temperature in water.

In this paper, we report on reversible self-assembly of a novel type of building blocks, i.e., noncovalently connected amphiphiles (NCCA) based on PNIPAM. For this purpose, cyclodextrin-ended PNIPAM and a hydrophobic dendron[19] with an azo group at the apex are synthesized. The hydrophilic PNIPAM chains could be capped with the hydrophoblic dendrons driven by the host−guest interactions between the cyclodextrin ends and the azobenzene groups. The formed NCCA is able to self-assemble into vesicles in water. Furthermore, the photoswitchable azo−cyclodextrin interactions result in reversibility of the assembly. In addition, the thermal-induced coil−globule transition of the PNIPAM chains leads to a thermo-stimuli response of the assembled objects. So dual-responsive assemblies are realized from the PNIPAM-based NCCA.

*Corresponding author. E-mail: mjiang@fudan.edu.cn.

## Results and Discussion

**Synthesis.** We designed and synthesized functionalized Frechét-type benzyl ether dendrons of generations of 1, 2, and 3 (G*x*-Azo, $x = 1$, 2, and 3) with an azobenzene group at the apex site (Scheme 1). The precursor dendrons of generation 1, 2, and 3 (G1, G2, and G3) were prepared according to the literature.[16,20] As shown in Scheme 1, for G1-Azo, 3,5-dihydroxylbenzoic acid (**1**) was used as starting material; after a three-step synthesis we successfully obtained bromo-substitute dendron **5** at the apex. Then (*E*)-4-(phenyldiazenyl)phenol was employed as a nucleophilic reagent to attack **5**, leading to the target molecule G1-Azo **6** in high yield after simple purification by column chromatography. The $^1$H NMR spectrum of G1-Azo is shown in Figure 1. The details of the synthesis procedure of G*x*-Azo ($x = 1$, 2, and 3) are described in the Experimental Section. The azo head in G1-Azo, as expected, shows perfect reversible isomerization in THF solutions by repeated alternating irradiation of UV (365 nm) and visible light (434 nm). This process was monitored by UV/vis spectroscopy, and the results are shown in the Supporting Information (Figure S2a,b).

The host polymer, linear PNIPAM modified with β-CD at one of the two ends (β-CD-PNIPAM), was prepared by atom transfer radical polymerization (ATRP). The key point in preparing β-CD-PNIPAM is the synthesis of the ATRP initiator, i.e., monosubstituted β-CD **18**. By carefully controlling


Published on Web 09/18/2009

**Scheme 1. Synthesis of G1-Azo**[a]

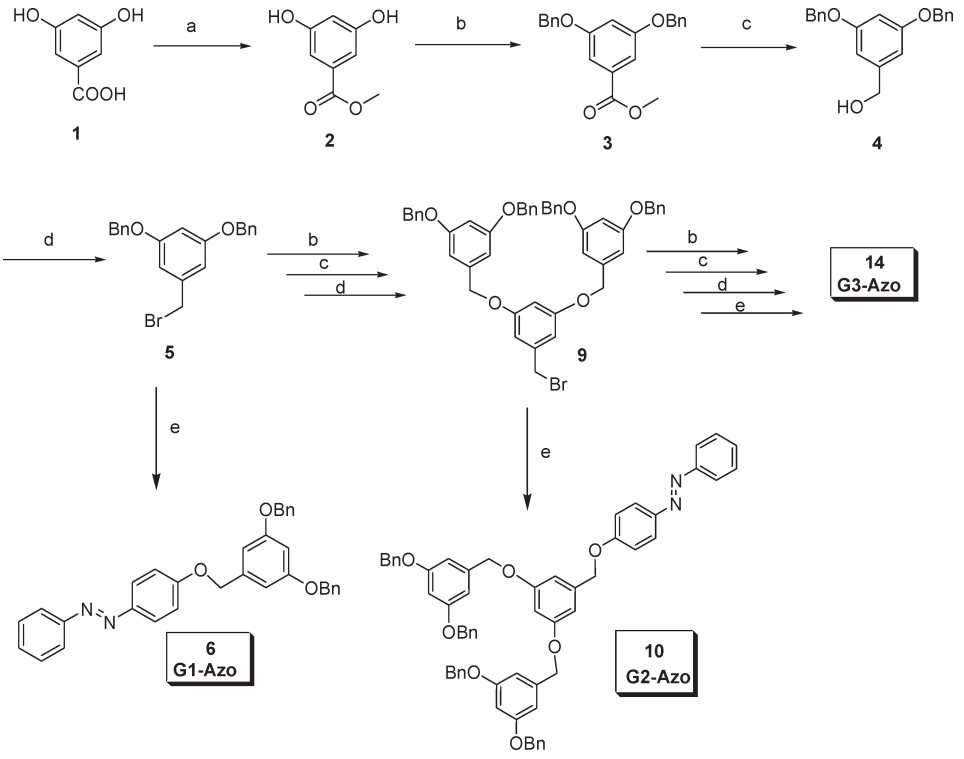


[a] Reagents and conditions: (a) $NaHSO_4 \cdot H_2O$, MeOH, reflux; (b) BnCl, $K_2CO_3$, [18]C-6, acetone, reflux; (c) $LiAlH_4$, THF, reflux; (d) $CBr_4$, $PPh_3$, THF, RT; (e) 4-(phenyldiazenyl)phenol, $K_2CO_3$, acetone, reflux.

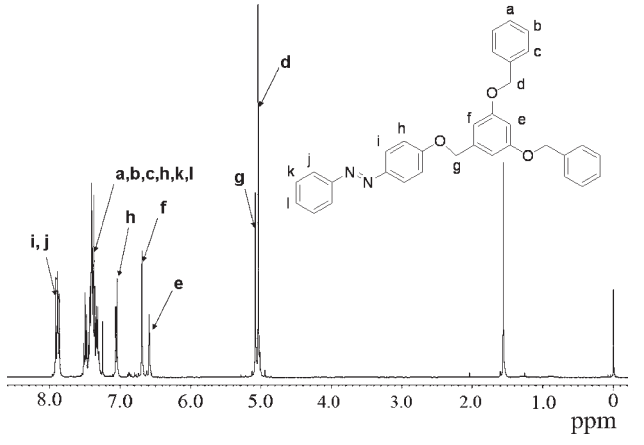


**Figure 1.** $^1$H NMR spectrum ($CDCl_3$) of G1-Azo.

the reaction conditions, we succeeded in obtaining initiator **18** (Scheme 2), which was confirmed by $^1$H NMR, $^{13}$C NMR, FT-IR, and MALDI-TOF measurements (Experimental Section). **18** was proved to be an efficient initiator in conjunction with tris[2-(dimethylamino)ethyl]amine ($Me_6$TREN) as a ligand. Such an initiator−catalyst system rendered the ATRP polymerization process efficiently in DMF leading to narrow dispersed $\beta$-CD-PNIPAM ($M_w/M_n = 1.46$, $M_w = 1.05 \times 10^4$ g/mol) according to gel permeation chromatography (GPC) results. The number-average molecular weight obtained from $^1$H NMR was $1.4 \times 10^4$ g/mol (Figure S1).

**Self-Assembly of the NCCA.** After screening most of ordinary organic solvents, THF was selected as a common solvent to dissolve both G1-Azo and $\beta$-CD-PNIPAM. First we mixed desired amounts of G1-Azo solution (1 mg/mL) and $\beta$-CD-PNIPAM solution (1 mg/mL) in THF to give molar ratios of G1-Azo/$\beta$-CD-PNIPAM ranging from 1:4 to 4:1. Then 0.1 mL of the mixed solution was quickly injected into 2 mL of water at 10 °C. Bluish opalescence appeared immediately, which indicated the formation of assembled particles. It is well-known that the azobenzene group as a guest can be included into the cavity of $\beta$-CD forming inclusion complexation in water.[21] This interaction enables the PNIPAM chains to be capped with hydrophobic dendrons resulting in an amphiphile and further assembled into nanopartcles. Dynamic light scattering (DLS) was employed to measure the sizes and size distributions of the particles. The DLS results (Table 1) show that over a broad molar ratio range of G1-Azo/$\beta$-CD-PNIPAM from 4:1 to 1:4 the mixture could form nanoparticles with average hydrodynamic radius ($R_h$) ranging from 60 to 110 nm. In this work, we focus on the nanoparticles with ratios of G1-Azo/$\beta$-CD-PNIPAM 1:1 (sample **a**) and 4:1 (sample **b**). The particles were very stable as a size increase was only observed by DLS after about 60 days standing. In addition, in the final dispersion of the nanoparticles the medium volume composition is THF/water 1/20. Dialysis of the solutions against water to remove THF was found to have little effect on the particle size. So the DLS measurements reported in this work were carried out for the solutions without dialysis.

Transmission electron microscopy (TEM) was used to exam the morphology of **a** and **b**. Figure 2 shows that in both cases the particles are spherical with diameters ranging from 100 to 200 nm, which is in accordance with the results given by DLS measurements. More importantly, the particles show a clear contrast between the center and the periphery, which is typical of vesicular structures.

A close examination of AFM of sample **b** in tapping mode (Figure 3) clarifies detailed morphology of the thin layer vesicles. Both the height and phase images show round outline shapes. A typical particle shows a horizontal distance of 139 nm similar to the diameters observed by TEM.

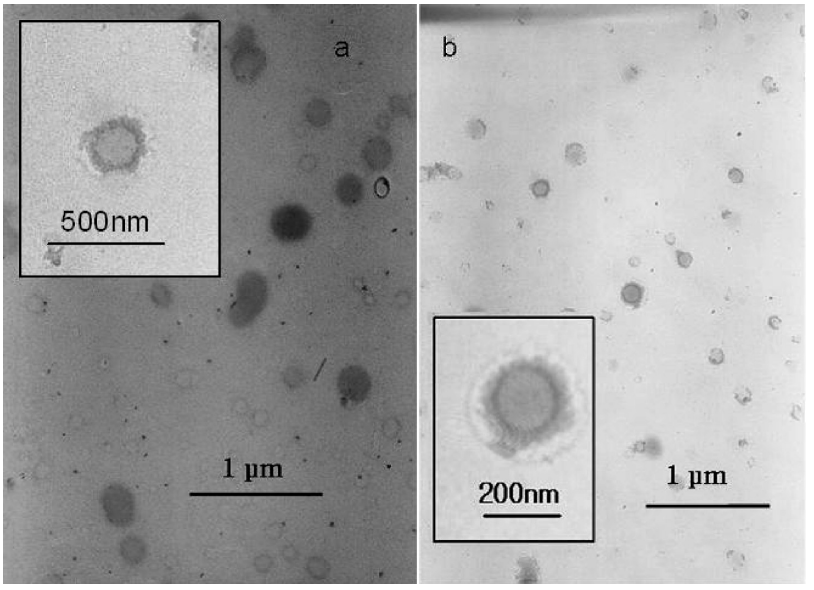


**Figure 2.** TEM images of the aggregates of sample **a** (a) and sample **b** (b).



**Scheme 2. Synthesis of β-CD-PNIPAM**

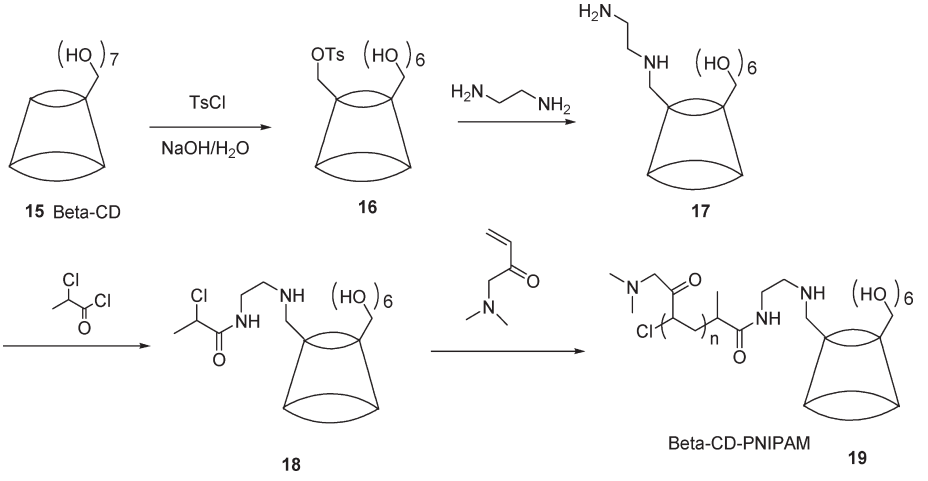


**Table 1. DLS Results of Aggregates Composed of G1-Azo and β-CD-PNIPAM at Different Molar Ratios**

| G1-Azo/β-CD-PNIPAM | 4:1 (**b**) | 2:1 | 1:1 (**a**) | 1:2 | 1:4 |
|---|---|---|---|---|---|
| $\langle R_h \rangle$/nm | 91.9 | 90.8 | 113.3 | 68.7 | 61.9 |
| PDI/$\mu_2/\langle \Gamma \rangle^2$ | 0.17 | 0.14 | 0.13 | 0.13 | 0.25 |

This indicates that the particles did not spread on the substrate. However, the height of the aggregates was found around 10 nm only, 1 order of magnitude smaller than the average diameter. This provides clear evidence of the hollow structure as such thin cakes can only be formed from collapsed thin wall of hollow spheres.[16]

The hollow structure is obviously caused by the self-assembly of the NCCA consisting of hydrophilic linear polymers PNIPAM and hydrophobic dendrons in water. $^1$H NMR measurements also support our assumptions on the structure of the aggregates (Figure 4). When THF-$d_8$ was used as a common solvent, both the dendron and β-CD-PNIPAM can be dissolved. Spectrum A of the mixture of G1-Azo/β-CD-PNIPAM 4/1 in THF-$d_8$ shows that the chemical shifts of azobenzene do not change compared to that of G1-Azo alone in THF-$d_8$ (Figure S3), which indicates no inclusion complexation between the azobenzene apex and β-CD end of PNIPAM in THF. Besides, due to the insolubility in THF, the β-CD group is expected to be buried within the PNIPAM coil which prevents its complexation with the azo groups. However, in $^1$H NMR spectrum B for aggregates **b** in THF-$d_8$/$D_2O$, v/v 1/20, the signals around 6.7−7.8 ppm associated with dendron and azobenzene decreased sharply while the signals of PNIPAM around 3.8 and 1.0 ppm changed a little. The results clearly show that the dendron units including the azo groups are in the aggregated state losing their mobility while all the PNIPAM chains, as the shell of the aggregates, remain in a soluble state.

On the basis of all the results discussed above, we propose a sandwich model for the vesicle membrane as shown in Scheme 3. In this model, the hydrophilic PNIPAM chains form both outer and inner layers facing water phase and the two layers are bridged by a hydrophobic layer of the compact dendrons (Scheme 3).

We made a rough estimation for the thickness of the vesicular membrane. From Chem3D the molecular size of G1-Azo is about 2.0 nm. The calculated average diameter of PNIPAM coils with $M_w$ of $1.05 \times 10^4$ g/mol in water is 4.4 nm.[22] So the thickness of the sandwich membrane in water is around 11 nm.

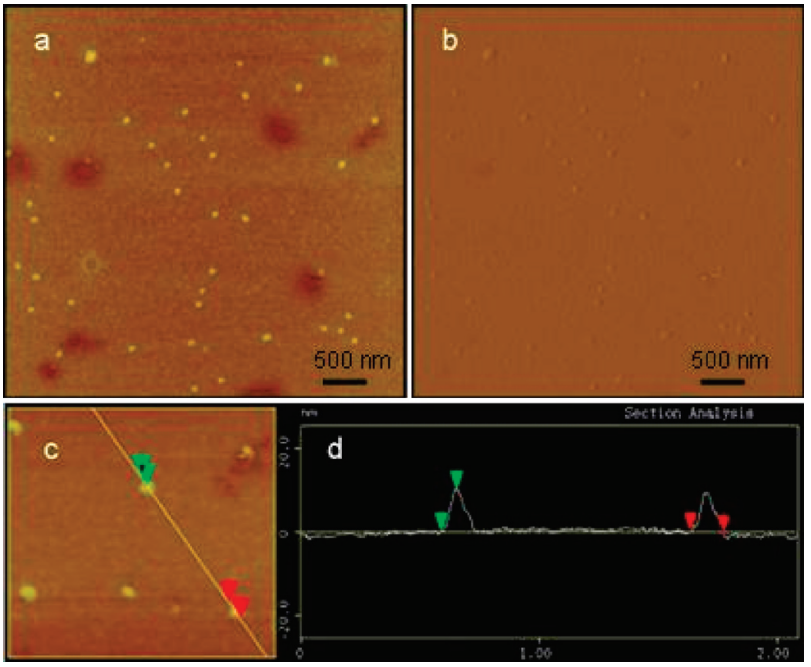


**Figure 3.** (a) Height and (b) phase AFM images of aggregates **b**. (c, d) AFM scan line giving horizontal distance 139.4 nm and vertical distance 10.0 nm.

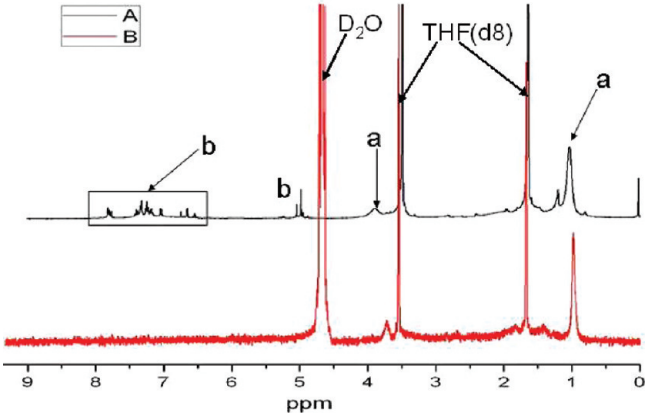


**Figure 4.** $^1$H NMR spectra of G1-Azo/$\beta$-CD-PNIPAM 4/1 in (A) THF and (B) THF-$d_8$/$D_2O$, v/v 1/20. a: PNIPAM signals; b: G1-Azo signals.

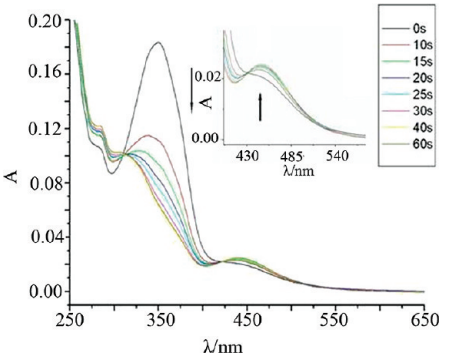


**Figure 5.** UV/vis spectra of sample **b** for increasing durations of UV irradiation ($\lambda$ = 365 nm) of 0, 10, 15, 20, 25, 30, 40, and 60 s (shown from the top down). The visible region is shown enlarged in the inset, for UV irradiation of 0, 10, 15, 20, 25, 30, 40, and 60 s (from the bottom up).

**Scheme 3. Schematic Illustration of the Vesicular Structure**

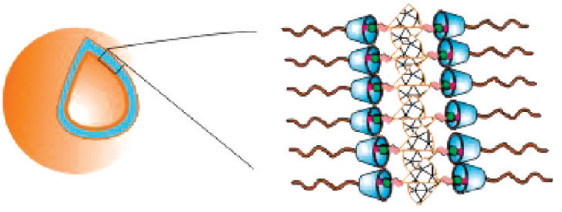

However, the height of the two overlapping membrane observed by AFM is only 10 nm. This apparent discrepancy seems understandable if the effects of the shrinkage of the PNIPAM chains and the deformation of the soft surface caused by the AFM tip in the height measurements are considered.[23,24]

**Reversibility of the Assembly.** Taking full advantages of the noncovalent connection between the azo head and $\beta$-CD and the optical switching properties of the inclusion complexation, we succeeded in realizing reversible self-assembly and disassembly of the NCCA. As shown in Figure 5, UV irradiation at 365 nm of the vesicles **b** at room temperature caused a substantial change in the UV/vis spectra. The absorption band at around 350 nm decreased gradually as the irradiation went on. Meanwhile, the band at around 440 nm increased slightly (inset, Figure 5). Because the absorption bands at 350 and 430 nm can be ascribed to $\pi-\pi^*$ of the trans form and $n-\pi^*$ of the cis form of the azo groups, respectively, this spectral variation clearly shows the isomerization of the azo group from the trans form to the cis form.

A remarkable change in the morphology of the aggregates caused by the UV irradiation was clearly visualized by TEM observations. As shown in Figure 6a, after 10 min of UV irradiation of sample **b**, which is coded as UV-**b**, the vesicular structure completely disappeared. Instead, a lot of solid spheres with a broad size distribution from 50 to 300 nm appeared, and some of the particles had irregular shapes, completely different from what is shown in Figure 2b for sample **b**. In tapping mode of the AFM measurement, large round spheres are present in both of the height and phase images (Figure 6b). Two typical round aggregates were measured, showing that the horizontal distances are as large as 600 nm and the respective vertical distances are 80 and 115 nm. The results indicate that the aggregates collapse and spread on the stages.

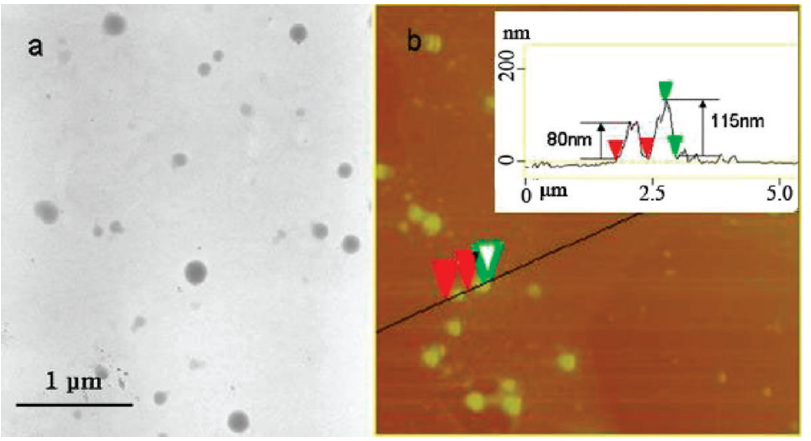


**Figure 6.** (a) TEM and (b) AFM images of the UV-irradiated aggregates of **b**. Horizontal (587 nm) and vertical (115 nm) distance analysis is shown in the inset.

**Table 2. DLS Results of the Aggregates for Sample b with Light Irradiation**

| sample | **b** | UV-**b** | vis−UV-**b** |
|---|---|---|---|
| $\langle R_h \rangle$/nm | 91.9 | 83.5 | 80.4 |
| PDI/$\mu_2/\langle \Gamma \rangle^2$ | 0.17 | 0.37 | 0.11 |

The UV irradiation resulted in a much broader size distribution as the PDI increased from 0.17 to 0.37 (Table 2). In addition, sample UV-**b** was not stable as it tended to precipitate on standing for a few days. It is worth mentioning that, in a control experiment, adding a dilute solution of G1-Azo in THF to pure water led to aggregates with $\langle R_h \rangle$ as large as 414 nm and a broader size distributions (PDI 0.23). Thus, the behavior of UV-**b** is very similar to the aggregates made of the dendron alone in water. In other words, in UV-**b**, as the result of exclusion of the azo groups of the hydrophobic dendron from the cavities of $\beta$-CD, the dendrons formed unstable aggregates.

Afterward, UV-**b** was subjected to visible-light irradiation at 434 nm at room temperature. As shown in Figure 7, in the UV/vis spectra, the absorption band around 350 nm increased remarkably, and the band around 430 nm decreased slightly. These results indicate the reverse isomerization of cis to trans. The resultant nanoparticles (vis−UV-**b**) were examined by TEM and AFM. As shown in Figure 8a, all the spheres present a clear contrast between a dark periphery and a gray central part, typical of hollow spheres. Thus, the visible-light irradiation results in converting the solid particles to vesicles. AFM test also gave proof of the reassembled vesicles. As shown in Figure 8b,c, round particles with an average diameter around 170 nm and a hight of 12 nm can be regarded as collapsed thin layer hollow structure. The recovered vesicles had an average $\langle R_h \rangle$ of 80.4 nm, very similar to that of the original vesicles, and the PDI fell from 0.37 to 0.11 (Table 2). Therefore, all these data of AFM, TEM, and DLS/SLS suggested that under this visible light irradiation reorganization of the solid spheres of UV-**b** returning to vesicles took place. In other words, by successive UV and visible light irradiations we realized a perfect cycle of vesicles−solid spheres−vesicles of the NCCA.

**Effect of Dendron Generation on the Assembly.** We have discussed the assembly of the NCCA with the smallest cap, i.e., the first generation of the dendron (G1-Azo). It shows that even the hydrophobic cap is pretty small it is able to make the amphiphile assembled in water. In order to explore the effect of dendron generation on the self-assembly, the NCCAs of G$x$-Azo ($x$ = 2 and 3) were studied as well. The micellar preparation is the same as that for sample **b** of G1-Azo. For the

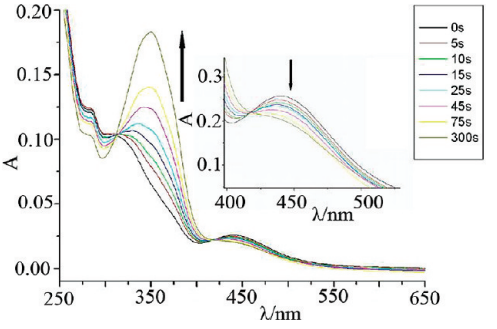


**Figure 7.** UV/vis spectra of UV-**b** (after 10 min of UV irradiation of sample **b**, which is coded as UV-**b**) for increasing durations of visible light irradiation ($\lambda$ = 434 nm) of 0, 5, 10, 15, 25, 45, 75, and 300 s (shown from the bottom up). The visible region is shown enlarged in the inset (from the top down).

case of G2-Azo, the TEM image of the resultant nanoparticles clearly displays hollow structure as shown in Figure 9a. The DLS measurement indicated that the radius of the particle is around 65 nm, which is in agreement with the TEM observations. In other words, using the first and second generations led to the similar results. However, for G3 and $\beta$-CD-PNIPAM, solid spheres rather than vesicles were observed in TEM images (Figure 9b). This morphological change caused by increasing the dendron generation seems understandable. With the raise of dendron's generation, the azo group is prone to be buried by the dendron bodies leading to a less opportunity entering into CD's cavity. Thus, the aggregates prefer solid spheres to vesicles as the former has much smaller surface area than the vesicles.

**Temperature-Responsive Behavior of the Assemblies.** It is well-known that PNIPAM chains in water solutions exhibit a reversible coil−globule transition at their lower critical solution temperature (LCST) around 32 °C.[25] Even in the temperature range below but close to the LCST, increasing temperature may favor the chain conformation of PNIPAM with a higher hydrophobicity although they remain soluble. On the basis of this valuable character of PNIPAM, we succeeded in realizing a dual-stimuli responsive self-assembly of the NCCA. As shown in Figure 10, both the water solutions of $\beta$-CD-PNIPAM and the self-assembled sample **b** sharply turn to opaque without precipitation when the temperature increases to 32.8 °C for the former and 29.8 °C for the latter. Thus, the solution of vesicles **b** displays an apparently lower LCST than that of $\beta$-CD-PNIPAM. It is known that the LCST of PNIPAM can be adjusted either by incorporating a comonomer by covalent bonds[26] or by inducing a guest molecule through noncovalent interactions.[27]

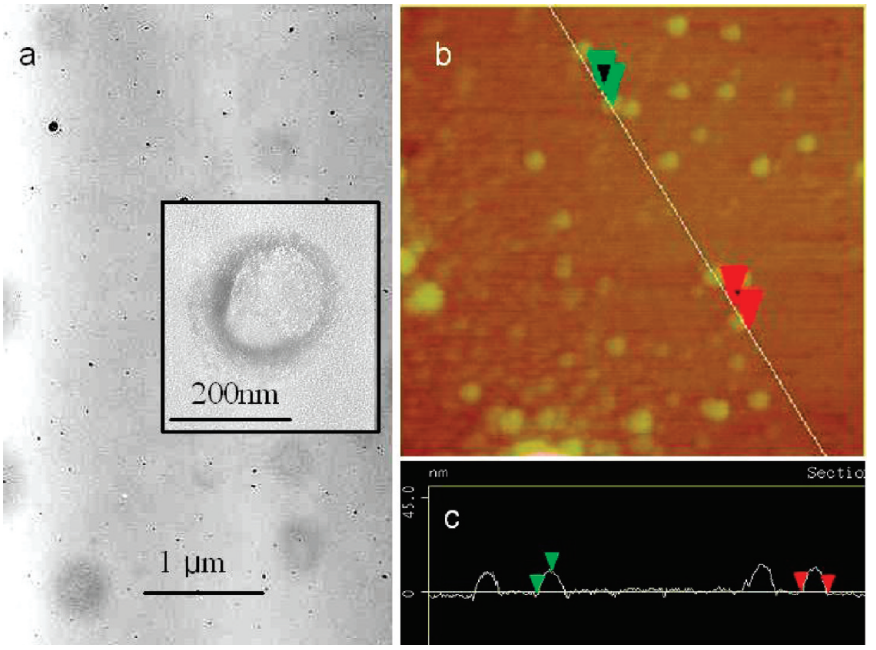


**Figure 8.** (a) TEM images of vis−UV-**b**. (b) AFM images of the aggregates of UV-**b** showing (c) horizontal distance 159.6 nm and vertical distance 11.7 nm.

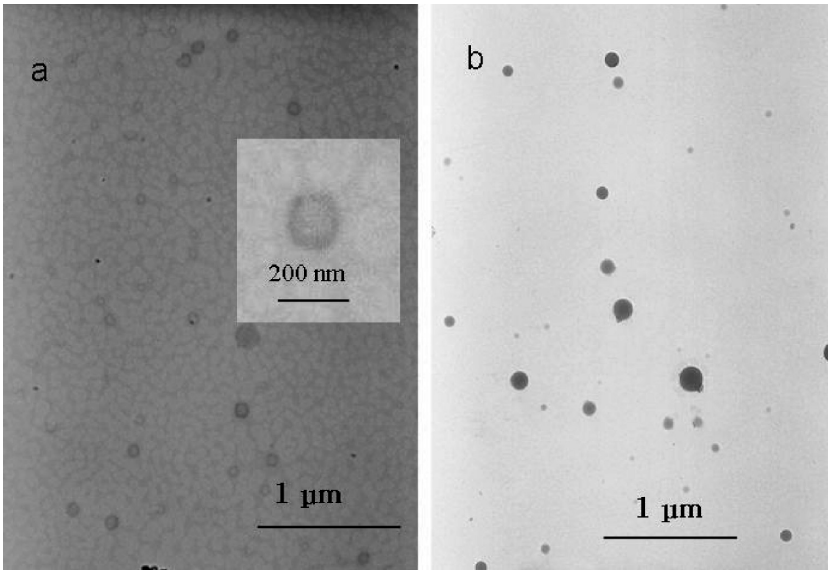


**Figure 9.** TEM images of self-assembled aggregates of $\beta$-CD-PNIPAM with (a) G2-Azo and (b) G3-Azo.

Clearly, in the present case the lower LCST of the vesicles compared to that of $\beta$-CD-PNIPAM can be attributed to the hydrophobic Azo-dendron which connected to the PNIPAM chains through the inclusion complexation.

DLS was used to monitor the heat response of the solutions of vesicles **b**. In the curve of aggregate size vs temperature (Figure 11), the most remarkable feature is the dramatic increase of $\langle R_h \rangle$ from 60 to 807 nm in a small temperature range from 30.5 to 31.6 °C. This is obviously attributed to the fact that above the LCST the coil PNIPAM chains in the vesicles turn to globules, which makes the vesicle instable. The vesicles tend to combine each other further forming larger aggregates. It is interesting to see that during the heating process, before the vesicle aggregation, there is a small but clear decrease of the vesicles from 82.7 nm at 29 °C to 60 nm at 30.5 °C (Figure 11b). As indicated by the turbidity change with temperature (Figure 10), the coil−globule transition of PNIPAM chains starts at 29 °C. This of course results in intrachain collapse on the surface of the vesicles leading to the size drop. As the temperature increases further, the hydrophilicity of vesicular surface is getting worse and worse, the interchain collapse from the shrank vesicles takes place, and thus larger aggregates form to reduce the total surface energy. When the temperature reaches 32 °C, the aggregate size no longer increases with temperature. Some typical DLS size distribution curves of the vesicles **b** with increasing temperature are shown in Figure 12. Curve A refers to the original vesicles. Curve B shows the average size decrease at the initial stage of the temperature increase. An apparent size increase is shown in curve C, indicating aggregation of the vesicles. And finally, in curve D, the size reaches its plateau of 830 nm when temperature increases to 32.9 °C. It is worth noting that when the aggregate solutions were cooled from 34 °C gradually to 25 °C, we observed a size decrease, and it finally returned to its original

value (Figure 11). Thus, this temperature response of the vesicles is proved to be reversible. However the size dramatic decrease in the cooling process takes place at 26−27 °C, which is much lower than that for the size quick increase in heating process. It may imply that the disaggregation of the second aggregates needs disentanglement of the collapsed PNIPAM chains on the surfaces of different vesicles, which is obviously difficult kinetically.

Very similar size variation with increasing temperature was observed for vesicles **a** with the ratio G1-Azo/$\beta$-CD-PNIPAM = 1:1 (Figure S4). The dramatic size changes take place in narrow temperature ranges of 31−32 °C and 29−30 °C on heating and cooling of the solutions, respectively.

SEM observations (Figure 13a) for sample **a** after the temperature increased to 34 °C clearly show the formation of larger aggregates with diameters around 1 $\mu$m. It is interesting to see that all the particles have irregular outline which may indicate that the particles were resulted by second aggregation of the original vesicles. Similar results were obtained for sample **b** (Figure S5). This explanation is confirmed by our TEM observations. As shown in Figure 13b, all the large aggregates have irregular shape, and each of them is composed of a few vesicles. In other words, when the vesicles aggregate each other due to increasing temperature, the vesicles did not change their own structure. In fact, the TEM observations also explored that the aggregates returned to individual vesicles as the heated sample **a** was cooled to 25 °C (Figure 13c). All the particles display clear circles with thin wall. The size of the vesicles is in the range in good agreement with DLS measurements (curve for 24.05 °C, Figure S6). Some typical DLS size distribution curves of the vesicles **a** with increasing and decreasing temperature are shown in Figures S6 and S7, respectively.

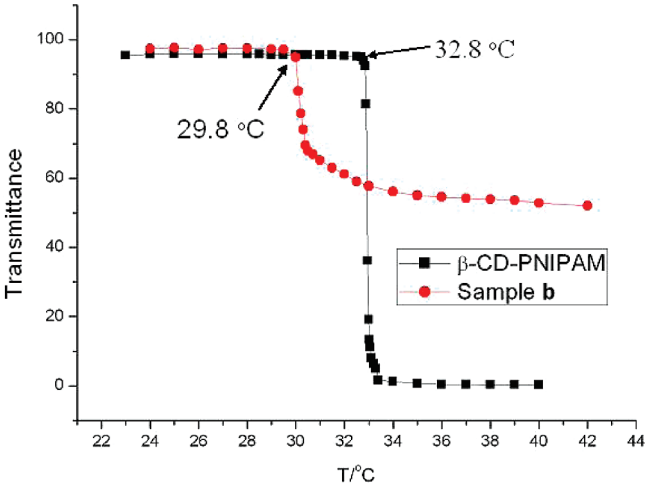


**Figure 10.** Turbidity changes of aqueous solution of $\beta$-CD-PNIPAM and sample **b** with increasing temperature.

## Experimental Section

**Materials.** All materials and reagents were obtained from commercial suppliers for direct use unless mentioned. 3,5-Dihydroxybenzoic acid (97%, Alfar), [18]crown-6 ([18]C-6; 99%, Acros), lithium tetrahydroaluminate ($LiAlH_4$; typically 97%, Alfar), carbon tetrabromide ($CBr_4$; 99%, Shanghai Chemicals), *p*-toluenesulfonic chloride (TsCl; 99%, Shanghai Chemicals), anhydrous potassium carbonate ($K_2CO_3$; AR, Shanghai Chemicals), benzyl chloride (BnCl; CP, Shanghai Chemicals), triphenylphosphine ($PPh_3$; CP, Shanghai Chemicals), and 4-(phenyldiazenyl)phenol (98%, Shanghai Chemicals). $\beta$-CD (CP, Shanghai Chemicals) was recrystallized twice from water. Ethane-1,2-diamine (99%, Shanghai Chemicals) and *N*-isopropylacrylamide (97%, Aldrich) were recrystallized twice from benzene/hexane (65:35 v/v) prior to use. Copper(I) chloride (97%, Shanghai Chemicals) and 2-chloropropanoyl chloride (97%, Alfar) were used as received. $Me_6TREN$ was prepared as described in the literature.[28]

**Characterization Methods.** A ALV/5000E laser light scattering (LLS) spectrometer was used. LLS measurements were

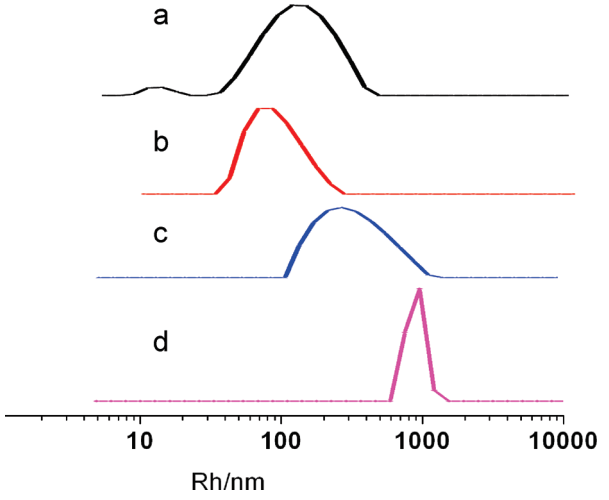


**Figure 12.** Changes of hydrodynamic radius $\langle R_h \rangle$ distributions of the sample **b** aggregates with increasing temperature: (a) 25.67 °C, $R_h$ = 93.18 nm; (b) 30.51 °C, $R_h$ = 59.96 nm; (c) 31.02 °C, $R_h$ = 281.24 nm; (d) 32.94 °C, $R_h$ = 830.30 nm.

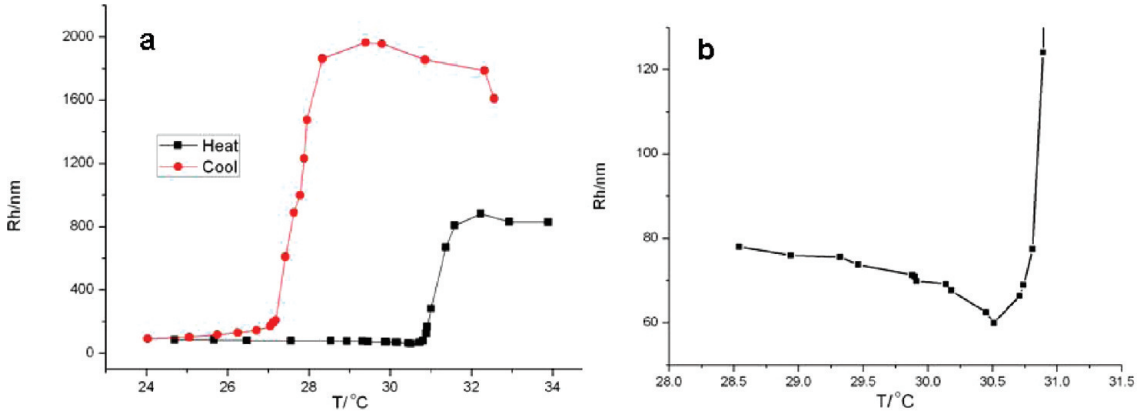


**Figure 11.** (a) Size changes of sample **b** with increasing and decreasing temperature and (b) the enlarged region showing the size change with temperature raise from 28.5 to 30.9 °C.

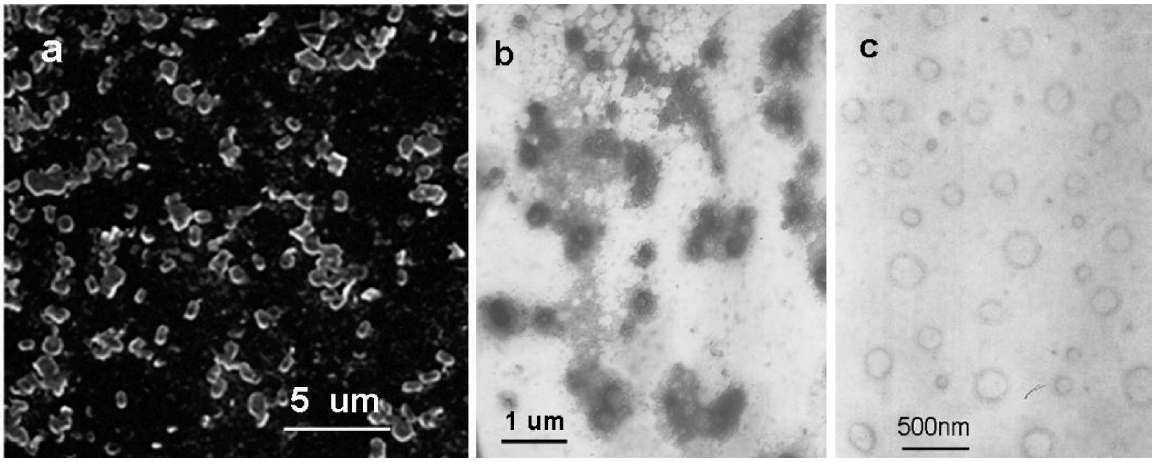


**Figure 13.** (a) SEM and (b) TEM images of sample **a** heated to 34 °C and (c) TEM image of sample **a** after a heating and cooling cycle.

**Scheme 4. Schematic Illustration of the Photoswitchable Self-Assembly and Disassembly and the Temperature-Responsive Properties of the NCCAs**

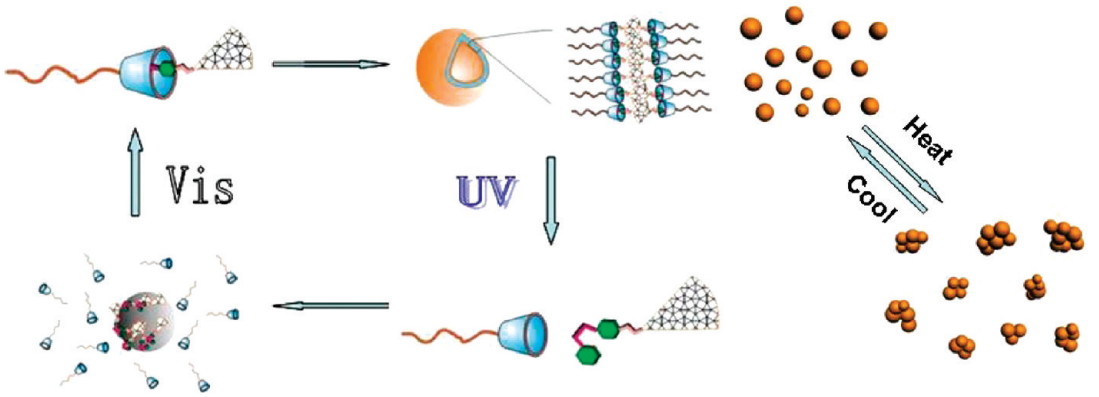




performed at a low concentration of 0.05 mg/mL at 25.0 ± 0.1 °C. As $\langle R_h \rangle$ values from DLS measured at 90° were used (Tables 1 and 2). The $\langle R_h \rangle$ and polydispersity index (PDI, $\mu_2/\langle\Gamma\rangle^2$) were obtained by a cumulant analysis. All the micelle solutions were measured directly without further dilution, and the solutions were cleaned using a 800 nm filter before measurements.

TEM observations were performed on a Philips CM 120 electron microscope at an accelerating voltage of 80 kV. A small drop from the micellar solutions kept at a given temperature was deposited onto preheated carbon-coated coppers EM grid and then dried at the same temperature.

The AFM images were acquired in tapping mode by using a Nanoscope IV from Digital Instruments equipped with a silicon cantilever with 125 ímand E-type vertical engage piezoelectric scanner. The sample preparation was similar to that for TEM, but new cleaved mica was used as the substrate.

The light transmittance of the micellar solutions was monitored at a fixed wavelength of 750 nm by means of a Perkin-Elmer Lamda 35 UV/vis spectrophotometer, equipped with a circulating water bath. For the cases of temperature-varying process, the operation was conducted with a programmed temperature increasing from 25 to 40 °C; the increasing rate was 1 °C/30 min.

UV irradiation was carried out with a CHF-XM35-500W (Beijing Changtuo Instrument Co.) high-pressure mercury lamp coupled with UV filters (365 nm, half-bandwidth 12 nm). $E$ = 2 mW/cm$^2$. Irradiation by visible light was performed using filters (434 nm, half-bandwidth 10 nm). $E$ = 0.2 mW/cm$^2$. UV/vis spectra were recorded on a Perkin-Elmer Lamda 35 UV/vis spectrophotometer.

$^1$H NMR (400 MHz) and $^{13}$C NMR (400 MHz) spectra were recorded by using a JEOL ECA-400 instrument. $CDCl_3$ and THF-$d_8$ were used as solvents and TMS as internal standard otherwise specified. Matrix-assisted laser desorption ionization time-of-flight (MALDI-TOF) mass spectra were recorded by using an Applied Biosystems Voyager-DE STR, using DCTB and THAP as the matrix, observing reflector-positive ions. β-CD-PNIPAM was characterized by gel-permeation chromatography (GPC, Agilent 1100) THF as eluent, 1.0 mL min$^{-1}$, 35 °C, Polymer Laboratories PL gel 5 μm mixed C column (molecular weight range 200−2000K).

**Synthesis of G*x*-Azo.** G1-Azo (**6**): Compound **5** (0.38 g, 1 mmol), 4-(phenyldiazenyl)phenol (0.20 g, 1 mmol), and $K_2CO_3$ (1.38 g, 10 mmol) were respectively added to the flusk; 10 mL of acetone was used as solvent. The resulting reaction mixture was heated at reflux for 14 h, after which TLC (PE/EA 3:1) confirmed completion. The reaction was cooled to room temperature and filtered. The solvent was removed in vacuum to give the crude product. Further purification was carried out by flash column chromatography using silica gel (PE/EA) to give an orange powder in 84% yield. G2-Azo (**10**): The procedure was similar to that for G1-Azo. The orange powder product was isolated in 98% yield upon column chromatography. G3-Azo (**14**): The procedure was similar to that for G2-Azo, and the product was isolated in 56% yield upon column chromatography.

**Synthesis of β-CD-PNIPAM.** EDA-CD (**17**) was synthesized as reported in ref 29. 2-Chloro-*N*-(2-(mono-6-amino-β-CD)ethyl)-propanamide (**18**): In a 25 mL flask, EDA-CD (**17**) (0.236 g, 0.2 mmol) was dissolved in 10 mL of dry DMF and cooled to 0 °C. Then 2-chloropropanoyl chloride (26 mg, 0.2 mmol)−DMF solution (10 mL) was added into the flask dropwise in 1 h under

protection of $N_2$. The reaction was stirred at 0−5 °C in $N_2$ for 36 h and monitored by thin-layer chromatography using a developing solvent of *n*-butanol, methanol, and pure water (5:1:1, v/v). After the reaction was complete, the solution was poured into 50 mL of acetone. The resulting precipitate was washed by acetone several times and dried under vacuum to give 2.3 g of crude product. The crude product was dissolved in water and was charged into an activated carbon column (26−35 mash) and eluted with i-PrOH/MeOH/$H_2O$. The product was recrystallized in water and acetone gave 0.12 g of white solid in the yield of 48%.

**ATRP of β-CD-PNIPAM (19).** To prepare PNIPAM with a target degree of polymerization of 100, NIPAM (1.12 g, 10 mmol), CuCl (0.01 g, 0.1 mmol), and initiator (**18**) (0.127 g, 0.1 mmol) were dissolved in 10 mL of dry DMF. Under liquid nitrogen freezing, the round-bottom flask fitted with a septum was pumped to high vacuum and filled with nitrogen for three times. Then $Me_6$TREN (0.023 g, 0.1 mmol) dissolved in 2 mL of dry DMF injected to the flask immediately in nitrogen. The reaction system was again pumped to high vacuum under freezing and then purged with nitrogen for several times. After that the reaction system was pumped to high vacuum and be heated to 15 °C. The reaction was carried out at 15 °C under a slight positive pressure of nitrogen for 11 h. The reaction mixture was then quenched by adding THF and passed through a short silica column to remove the catalyst. Most of the solvent was removed under vacuum, and then 20 mL of $Et_2O$ was added to give a white solid. The crude product was dissolved in DMF and poured into $Et_2O$ twice. The molecular weight (PDI = 1.46, $M_w = 1.05 \times 10^4$ g/mol) of the product was determined by GPC analysis using PS standard and THF eluent. $^1$H NMR spectroscopy is shown in Figure S1 (Supporting Information).

## Conclusions

Scheme 4 illustrates the main results of the work. Noncovalently connected amphiphiles (NCCA), in which the hydrophobic dendrons G*x*-Azo and hydrophilic β-CD-PNIPAM chains are connected by inclusion interaction between azobenzene groups and β-CD, self-assemble in water into thin-layer vesicles. The vesicular membrane has a sandwich structure with two PNIPAM layers facing water phase, which are bridged by a hydrophobic layer of the compact dendrons. UV irradiation makes isomerization of the azo groups from trans form to cis form, which causes decomplexation between the azo groups and β-CD leading to the disappearance of the vesicles and the formation of irregular particles of G*x*-Azo. Subsequent irradiation of the solutions with visible light leads to the reversed variation; i.e., the azo groups change to trans form and complexation takes place, and then the irregular particles return to vesicles. These photoswitchable vesicles are also sensitive to temperature. Increasing temperature to about 34 °C causes second aggregation of the vesicles to form large and irregular aggregates due to the coil−globule transition of the PNIPAM chains. Cooling the solutions to about 25 °C makes the large particles return to vesicles. In short, the noncovalently connected amphiphiles show reversible dual-stimuli responsive behavior, and the self-assembly and disassembly are controlled by the process of supramolecular chemistry.

**Acknowledgment.** This work is supported by the National Natural Science Foundation of China (NNSFC No. 20774021, 20834004), Ministry of Science and Technology of China (2009-CB930400), and Technology Committee of Shanghai Municipality (07DJ14004)

**Supporting Information Available:** Characterization data of the products in the synthesis, $^1$H NMR spectra of β-CD-PNIPAM, G1-Azo and G1-Azo/β-CD-PNIPAM, UV/vis spectra of G1-Azo under UV and Vis irradiation, size changes of **a** with temperature; SEM images of **b** heated to 34 °C, TEM images of **b** after a heating and cooling cycle, and changes of $R_h$ distributions of **a** with temperature. This material is available free of charge via the Internet at http://pubs.acs.org.

## References and Notes

(1) Schild, H. G. *Prog. Polym. Sci.* **1992**, *17*, 163–249.
(2) Wang, X. H.; Qiu, X. P.; Wu, Q. *Macromolecules* **1998**, *31*, 2972–2976.
(3) Heskins, M.; Guillet, J. E. *J. Macromol. Sci., Part A: Pure Appl. Chem.* **1968**, *2*, 1441–1455.
(4) Li, M.; Jiang, M.; Zhang, Y. X.; Fang, Q. *Macromolecules* **1997**, *30*, 470–478.
(5) Nuopponen, M.; Ojala, J.; Tenhu, H. *Polymer* **2004**, *45*, 3643–3650.
(6) Schmid, H.; Michel, B. *Macromolecules* **2000**, *33*, 3042–3049.
(7) Leduc, M. R.; Hawker, C. J.; Dao, J.; Frechet, J. M. J. *J. Am. Chem. Soc.* **1996**, *118*, 11111–11117.
(8) Hawker, C. J.; Bosman, A. W.; Harth, E. *Chem. Rev.* **2001**, *101*, 3661–3668.
(9) Ge, Z. S.; Chen, D. Y.; Zhang, J. Y.; Rao, J. Y.; Yin, J.; Wang, D.; Wan, X. J.; Shi, W. F.; Liu, S. Y. *J. Polym. Sci., Part A: Polym. Chem.* **2007**, *45*, 1432–1445.
(10) Ge, Z. S.; Luo, S. Z.; Liu, S. Y. *J. Polym. Sci., Part A: Polym. Chem.* **2006**, *44*, 1357–1371.
(11) Li, G.; Shi, L.; An, Y.; Zhang, W.; Ma, R. *Polymer* **2006**, *47*, 4581–4587.
(12) Li, J. G.; Wang, T.; Wu, D. L.; Zhang, X. Q.; Yan, J. T.; Du, S.; Guo, Y. F.; Wang, J.; Zhang, A. F. *Biomacromelecules* **2008**, *9*, 2670–2676.
(13) Desponds, A.; Freitag, R. *Langmuir* **2003**, *19*, 6261–6270.
(14) Ju, X. J.; Liu, L.; Xie, R.; Niu, C. H.; Chu, L. Y. *Polymer* **2009**, *50*, 922–929.
(15) (a) Guo, M. Y.; Jiang, M. *Soft Matter* **2009**, *5*, 495–500. (b) Chen, D. Y.; Jiang, M. *Acc. Chem. Res.* **2005**, *38* (6), 494–502.
(16) Xie, D.; Jiang, M.; Zhang, G. Z.; Chen, D. Y. *Chem.—Eur. J.* **2007**, *13*, 3346–3353.
(17) (a) Andres, P. R.; Schubert, U. S. *Adv. Mater.* **2004**, *16*, 1043–1068. (b) Fustin, C. A.; Guillet, P.; Schubert, U. S.; Gohy, J. F. *Adv. Mater.* **2007**, *19*, 1665–1673. (c) Moughton, A. O.; O'Reilly, R. K. *J. Am. Chem. Soc.* **2008**, *130*, 8714–8725.
(18) (a) Liu, L.; Xu, J.; Craig, S. *Chem. Commun.* **2004**, 1864–1865. (b) Zeng, J.; Shi, K.; Zhang, Y.; Sun, X.; Zhang, B. *Chem. Commun.* **2008**, 3753–3755. (c) Zou, J.; Tao, F. G.; Jiang, M. *Langmuir* **2007**, *23*, 12791–12794.
(19) (a) Rudick, J. G.; Percec, V. A. *Acc. Chem. Res.* **2008**, *41*, 1641–1652.(b) *Dendrimers and Other Dendritic Polymers*; Fréchet, J., Tominia, D., Eds.; John Wiley & Sons Ltd.: New York, 2001. (c) Newkome, G.; Moorefield, C.; Vögtle, F. *Dendrimers and Dendrons*; Wiley-VCH: Berlin, 2002.
(20) Hawker, C. J.; Fréchet, J. M. J. *J. Am. Chem. Soc.* **1990**, *112*, 7638–7647.
(21) (a) Lahav, M.; Ranjit, K. T.; Katz, E.; Willner, I. *Chem. Commun.* **1997**, 259–260. (b) Liu, Y.; Zhao, Y. L.; Zhang, H. Y.; Fan, Z.; Wen, G. D.; Ding, F. *J. Phys. Chem. B* **2004**, *108*, 8836–8843. (c) Sanchez, A. M.; Rossi, R. H. *J. Org. Chem.* **1996**, *61*, 3446–3451. (d) Liu, Z.; Jiang, M. *J. Mater. Chem.* **2007**, *17*, 4249–4254.
(22) Note: the average radius of gyration ($R_g$) of a long flexible polymer chains in a good solvent at low concentrations is proportional to $M_w^{0.6}$: $R_g \propto M_w^{0.6}$. Li et al. reported that $R_g$ = 46 nm for PNIPAM with $M_w = 7.7 \times 10^5$ in aqueous solution at 25 °C (see: Li, M.; Wu, C. *Macromolecules* **1999**, *32*, 4311−4316). Thus, the average diameter of the present PNIPAM in solution is about 4.4 nm.
(23) (a) Hansma, H. G.; Vac, J. *J. Vac. Sci. Technol., B* **1996**, *14*, 1390–1394. (b) Tamayo, J.; Garacia, R. *Langmuir* **1996**, *12*, 4430–4435.
(24) Yang, M.; Wang, W.; Yuan, F.; Zhang, X. *J. Am. Chem. Soc.* **2005**, *127*, 15107–15111.
(25) Zhang, G. Z.; Wu, C. *Adv. Polym. Sci.* **2006**, *195*, 101–176.
(26) Kawasaki, H.; Sasaki, S.; Maeda, H. *J. Phys. Chem. B* **1997**, *101*, 5089–5093.
(27) Ohashi, H.; Hiraoka, Y.; Yamaguchi, T. *Macromolecules* **2006**, *39*, 2614–2620.
(28) Ciampolini, M.; Nardi, N. *Inorg. Chem.* **1966**, *5*, 41–44.
(29) Liu, Y. Y.; Fan, X. D.; Gao, L. *Macromol. Biosci.* **2003**, *3*, 715–719.